FULL PAPER

Drug Delivery

ADVANCED
FUNCTIONAL
MATERIALS

www.afm-journal.de

Effective and Selective Anti-Cancer Protein Delivery via All-Functions-in-One Nanocarriers Coupled with Visible Light-Responsive, Reversible Protein Engineering

Hua He, Yongbing Chen, Yongjuan Li, Ziyuan Song, Yinan Zhong, Rongying Zhu, Jianjun Cheng,* and Lichen Yin*

Efficient intracellular delivery of protein drugs and tumor-specific activation of protein functions are critical toward anti-cancer protein therapy. However, an omnipotent protein delivery system that can harmonize the complicated systemic barriers as well as spatiotemporally manipulate protein function is lacking. Herein, an "all-functions-in-one" nanocarrier doped with photosensitizer (PS) is developed and coupled with reactive oxygen species (ROS)-responsive, reversible protein engineering to realize cancer-targeted protein delivery, and spatiotemporal manipulation of protein activities using long-wavelength visible light (635 nm) at low power density (5 mW cm^{-2}). Particularly, RNase A is caged with H_2O_2-cleavable phenylboronic acid to form 4-nitrophenyl 4-(4,4,5,5-tetramethyl-1,3,2-dioxaborolan-2-yl)benzyl carbonate (NBC)-modified RNase (RNBC), which is encapsulated in acid-degradable, ketal-crosslinked PEI (KPEI)-based nanocomplexes (NCs) coated with PS-modified hyaluronic acid (HA). Such NCs harmonize the critical processes for protein delivery, wherein HA coating renders NCs with long blood circulation and cancer cell targeting, and KPEI enables endosomal escape as well as acid-triggered intracellular RNBC release. Tumor-specific light irradiation generates H_2O_2 to kill cancer cells and restore the protein activity, thus achieving synergistic anti-cancer efficacy. It is the first time to photomanipulate protein functions by coupling ROS-cleavable protein caging with PS-mediated ROS generation, and the "all-functions-in-one" nanocarrier represents a promising example for the programmed anti-cancer protein delivery.

1. Introduction

Protein drugs are highly valuable for therapeutic applications because of their pharmacological potency and selectivity.[1] Mounting evidences have revealed that many diseases arise from the dysfunction of intracellular proteins, and thus protein drugs targeting intracellular biological activities hold promising utilities for the treatment of human diseases, such as cancer.[2] However, to fully realize the vast anti-cancer potential of protein drugs in vivo, there are two major challenges that need to be perfectly addressed.[3] The first challenge is related to the targeted protein delivery into cancer cells. Proteins are prone to be rapidly degraded/inactivated in the serum upon systemic administration, and minimal amount of the protein can be accumulated in the tumor in its integral and active form.[4] Additionally, most protein drugs are impermeable to cell membranes due to their hydrophilicity and large size, leading to minimal uptake by cancer cells.[2b,5] With the attempt to maximize the anti-cancer efficacy of protein drugs while minimize their nonspecific side effects to normal cells,

H. He, Y. Li, Prof. L. Yin
Jiangsu Key Laboratory for Carbon-Based
Functional Materials and Devices
Institute of Functional Nano and Soft Materials (FUNSOM)
Joint International Research Laboratory of Carbon-Based
Functional Materials and Devices
Soochow University
Suzhou 215123, China
E-mail: lcyin@suda.edu.cn

Prof. Y. Chen, R. Zhu
Department of Cardiothoracic Surgery
the Second Affiliated Hospital of Soochow University
Suzhou 215004, China

Dr. Z. Song, Prof. J. Cheng
Department of Materials Science and Engineering
University of Illinois at Urbana-Champaign
Urbana, IL 61801, USA
E-mail: jianjunc@illinois.edu

Dr. Y. Zhong
Biomedical Polymers Laboratory and Jiangsu Key Laboratory
of Advanced Functional Polymer Design and Application
College of Chemistry
Chemical Engineering and Materials Science
Soochow University
Suzhou 215123, China

**ADVANCED
SCIENCE NEWS**
www.advancedsciencenews.com

**ADVANCED
FUNCTIONAL
MATERIALS**
www.afm-journal.de

it is desired that the critical functionality of protein drugs be masked in normal cells while be efficiently and spatiotemporally activated in cancer cells, which imposes another challenge for protein therapy.

To enhance the delivery efficiency of anti-cancer proteins, various nanocarriers, such as liposomes, solid lipid nanoparticles (NPs), polymeric NPs, inorganic NPs, and protein-based carriers, have been developed.[6] While the nanovehicles can prevent protein proteolysis in the biological environment, reduce renal filtration, and improve tumor accumulation, the cancer-targeted intracellular protein delivery still suffers from low efficiency, because the complicated systemic barriers pose conflicting requirements for the nanoproperties.[7] For instance, to enable improved pharmacokinetics, PEGylation of nanoparticle surface is the most commonly used approach, which concealed the antigenic epitopes to attenuate receptor-mediated uptake by the reticuloendothelial system (RES).[8] However, the hydrophilic PEG corona will conversely reduce the interaction with cancer cell membranes, thus impeding the uptake by cancer cells.[9] Upon internalization, the lack of an efficient endolysosomal escape mechanism also greatly hurdles the intracellular function of the protein cargo.[10] Another inconsistence is associated with the "on-demand" release of proteins in the cytosol. While stable encapsulation of proteins contributes to their enhanced stability during systemic transit, it at the meantime limits the intracellular protein release to hamper their anti-tumor activity.[6b,11] To the best of our knowledge, an omnipotent protein carrier that can harmonize all these conflicting delivery processes for cancer treatment is still lacking.

Reversible caging of proteins with trigger-cleavable motifs affords an appealing approach to manipulate the protein function inside cells. Varieties of internal stimuli-activatable proteins have been engineered, wherein the protein activity is inhibited at the caged state while is recovered after removal of the blockage moieties by intracellular stimuli such as acidic pH in the endolysosomes[12] and reactive oxygen species (ROS) overproduced in cancer cells.[13] However, noncancerous cells also possess acidic endolysosomes, thus leading to undesired toxicity in normal cells. The ROS-activatable protein, on the other hand, suffers from low anti-cancer potency because the ROS levels in cancer cells are often not high enough to efficiently cleave the ROS-responsive caging groups.[14] In comparison, controlling the protein activity with external triggers, such as light, has emerged as a powerful strategy to address such challenges. In particular, photomanipulation of protein functions features easy maneuverability, high spatiotemporal precision by controlling the light irradiation site, dose, and time, and minimal damage to normal tissues within the safe optical power range.[15] However, majority of the reported photocaged proteins is responsive to UV light, which suffers from low tissue penetration depth and photodamage to intracellular proteins, lipids, and nucleic acids. Because near-infrared (NIR) light irradiation features deep tissue penetration and low phototoxicity, proteins with two-photon-responsive caging groups have been developed.[16] Alternatively, UV-responsive proteins are also coupled with upconversion nanoparticles (UCNPs) which can be excited by multiple NIR photons to emit a single high-energy photon with shorter wavelength within the UV region.[17] Nevertheless, these approaches usually require light irradiation with high optical power densities (0.5–5 W cm^{-2}), which would cause heat damage to tissues and thus may not be suitable for in vivo use.[17a,18]

To overcome the aforementioned challenges, we herein for the first time realize the photomanipulation of protein activity by coupling a ROS-cleavable, reversibly caged anti-cancer protein drug with a photosensitizer (PS). PS generates high amount of ROS under tumor site-specific, long-wavelength visible light irradiation (635 nm) at low optical power density (down to 5 mW cm^{-2}), and thus restores the protein function (**Figure 1**). With the attempt to effectuate the targeted protein delivery into cancer cells, we further construct an "all-functions-in-one" nanocarrier with synchronized properties to harmonize all the critical delivery processes, such as blood circulation, tumor accumulation, cancer cell uptake, endolysosomal escape, and intracellular protein release.

In support of such design strategy, RNase A, a clinically used protein drug for treating refractory cancer,[19] was caged with H_2O_2-cleavable phenylboronic acid on its lysine residues to form the deactivated prodrug, 4-nitrophenyl 4-(4,4,5,5-tetramethyl-1,3,2-dioxaborolan-2-yl)benzyl carbonate (NBC)-modified RNase (RNBC) (Scheme S2, Supporting Information). Cationic, acid-degradable, ketal cross-linked polyethylenimine 600 Da (KPEI) was developed to form nanocomplexes (NCs) with RNBC via electrostatic interaction, which could enhance the protein stability and facilitate its cellular internalization. Hyaluronic acid (HA) conjugated with hematoporphyrin (Hp) as the PS (HA-Hp) was further coated onto the surface of NCs to enhance their serum stability due to shielding of the positive charges, thus enabling long circulation in the blood and promoting tumor accumulation due to the permeability and retention (EPR) effect. Unlike PEG that hampers the cellular internalization, HA promotes the cell uptake of NCs based on its affinity with overexpressed CD44 on cancer cell membranes. After internalization into cancer cells via CD44-mediated endocytosis, KPEI quickly degrades into low-molecular-weight (MW) segments in the acidic endolysosomes, which facilitates RNBC release and diminishes material toxicity associated with high MW. Meanwhile, KPEI mediates effective endosomal escape due to the "proton sponge" effect. Light irradiation of Hp then generates high levels of H_2O_2 to kill cancer cells (so-called "photodynamic therapy," PDT[20]), and simultaneously enables complete restoration of protein activity by cleaving the phenylboronic acid caging group, thus leading to synergistic anti-cancer effect (Figure 1).

2. Results and Discussion

2.1. Synthesis and Characterization of RNBC

PEI 600 Da was cross-linked by a pH-labile ketal linker to obtain KPEI with high MW (4302 Da) and cationic charge density (Scheme S1, Supporting Information). RNBC was synthesized via reaction of RNase A with NBC in NaHCO$_3$ solution (0.1 M, pH 8.5) followed by purification with ultrafiltration (Scheme S2A, Supporting Information).[13] The lysine residues in RNase A were thus partially caged with phenylboronic acid through a covalent carbamate linker. The conjugation efficiency
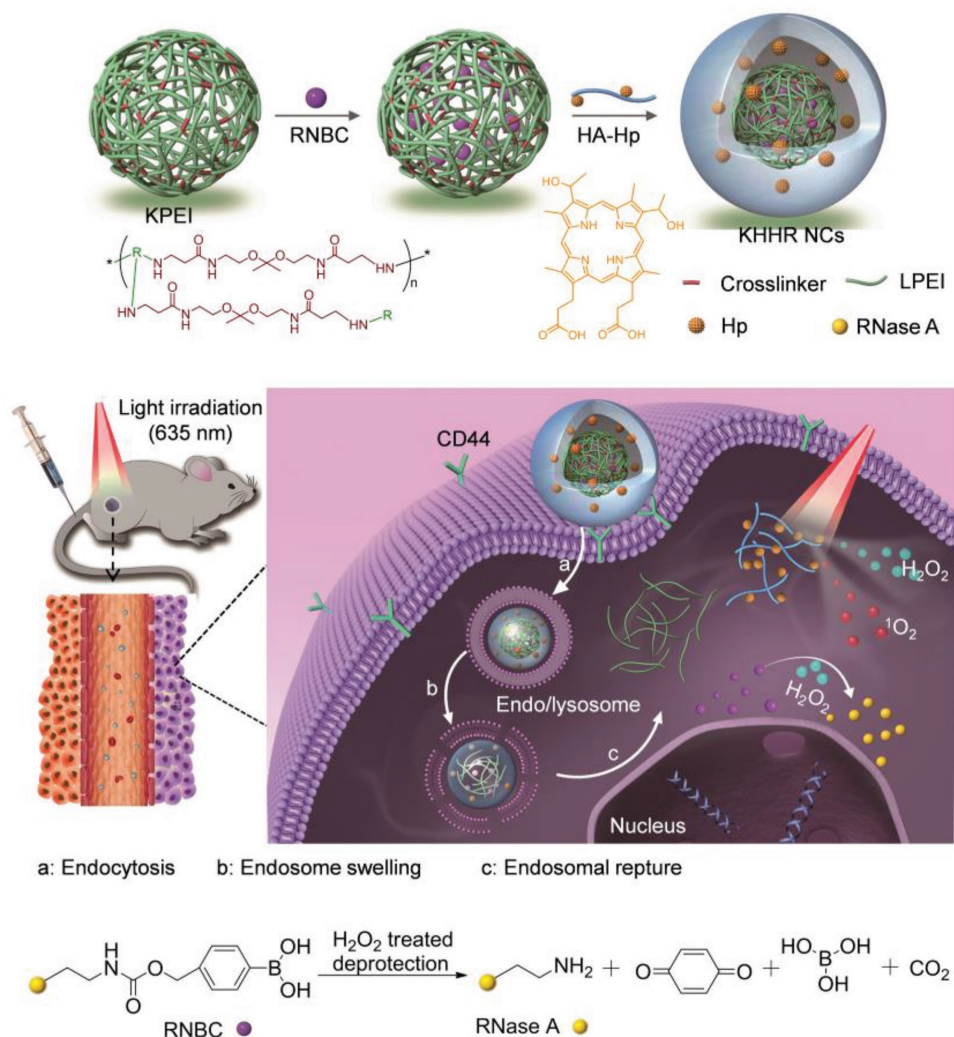
Figure 1. Schematic illustration of light-controlled protein delivery assisted by the "all-functions-in-one" nanocomplexes (NCs) toward synergistic cancer therapy. KHHR NCs were formed via the electrostatic interaction between phenylboronic acid-caged RNase A (RNBC) and ketal-crosslinked PEI (KPEI), which were further coated with HA-haematoporphyrin (HA-Hp) to feature high serum stability. Upon reaching the tumor tissues, KHHR NCs entered cancer cells via CD44-mediated endocytosis, released RNBC upon acid-triggered degradation of KPEI in the endosomes, and escaped the endosomes via KPEI-assisted "proton sponge" effect. Visible light irradiation (635 nm) of the PS at low power density (5 mW cm^{-2}) generated large amount of H$_2$O$_2$ to restore the activity of RNBC and subsequently exerted synergistic anti-cancer efficacy.

of NBC to RNase A was first characterized by the Alizarin Red S (ARS) assay, where the catechol moieties in ARS bind to the aryl boronic acid residues in RNBC to generate highly fluorescent complexes.[21] As shown in Figure S3 (Supporting Information), the ARS fluorescence was enhanced by 11-fold upon addition of RNBC while was negligibly altered upon addition of RNase A, which demonstrated the successful incorporation of NBC groups onto RNase A. MALDI-TOF analysis further revealed that the MW increased from 13 700 Da (RNase A) to 15 400 Da (RNBC), suggesting that seven NBC molecules were conjugated to one RNase A molecule (Figure 3C).

2.2. Preparation and Characterization of Nanocomplexes

After modification with NBC, the lysine groups were caged to diminish the positive charges on RNase A, and the conjugated

phenylboronic acid further endowed the protein with negative charges. Therefore, KPEI and RNBC were allowed to form NCs via electrostatic interactions. The KPEI/RNBC NCs (KR NCs, KPEI/RNBC = 15/1, w/w) showed particle size of ≈150 nm and positive surface charge of 8.9 mV. The drug loading content (DLC) of RNBC was 3.2%, and the drug loading efficiency (DLE) was 98.6%. HA-Hp was synthesized (Scheme S2B, Supporting Information) and was coated onto the surface of KR NCs via electrostatic interaction, yielding the KPEI/HA-Hp/RNBC NCs (KHHR NCs, KPEI/HA-Hp/RNBC = 15/15/1, w/w/w) with particle size of ≈170 nm and negative surface charge of −11.0 mV. Transmission electron microscopy (TEM) image also showed that KHHR NCs possessed spherical morphology with an average particle size of ≈140 nm, which was consistent with the dynamic laser scanning (DLS) measurement (Figure S4, Supporting Information). It was thus
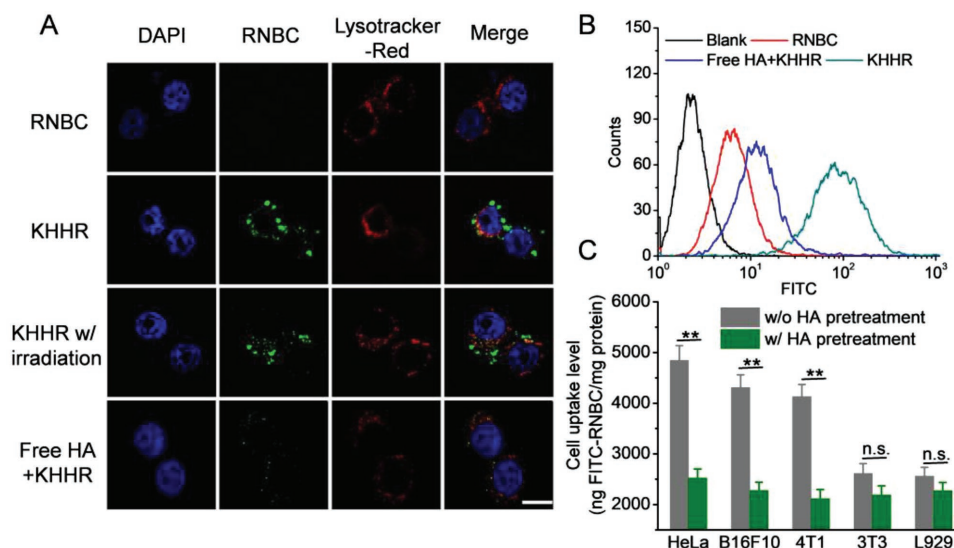
Figure 2. KHHR NCs mediated targeted delivery of RNBC into cancer cells in vitro. A) CLSM images of HeLa cells following incubation with KHHR NCs at 37 °C for 4 h and light irradiation (635 nm, 5 mW cm^{-2}) for 30 min. Cell nuclei were stained with DAPI and endosomes/lysosomes were stained with Lysotracker Red. Bar represents 15 μm. B) Uptake of RNBC and KHHR NCs in HeLa cells following 4 h incubation as evaluated by flow cytometry. HeLa cells were pre-treated with HA for 4 h to black CD44 and the HA-mediated targeting effect. C) Uptake level of KHHR NCs containing FITC-RNBC in various cell lines with or without pretreatment of free HA ($n = 3$).

suggested that HA coating shielded the positive surface charges of KR NCs while had slight effect on the particle size. After incubation with serum for 2 h, particle size of KR NCs remarkably increased while KHHR NCs remained desired stability (Figure S5A, Supporting Information), which indicated that HA coating could greatly enhance the stability of NCs by preventing adsorption of serum proteins and would thus provide implications for prolonged blood circulation in vivo. Considering that the extracellular compartment in the tumor microenvironment is slightly acidic (pH ≈ 6.8), we further evaluated the stability of NCs in PBS (pH 6.8) after incubation for up to 2 h. Consistently, particle size of KR NCs remarkably increased while KHHR NCs remained unaltered (Figure S5B, Supporting Information), which further suggested that the KHHR NCs possessed desired stability in the slightly acidic tumor microenvironment. In vitro release of RNBC was then monitored in PBS or acetate buffer at pH 7.4 and 5.0, respectively. As shown in Figure S6 (Supporting Information), RNBC release at pH 7.4 was negligible, leading to the accumulative release amount of 15.7% within 24 h. In comparison, RNBC was quickly released at pH 5.0, resulting in the accumulative release amount of 85.3% within 24 h. Such pH-responsive RNBC release profiles could be attributed to the degradation of the pH-responsive KPEI under acidic conditions, which would allow the NCs to effectively release RNBC in the acidic endolysosomes upon internalization into cancer cells (Figure S6, Supporting Information).

2.3. HA-Mediated Cancer Cell Targeting and Cellular Uptake

We then evaluated the HA-mediated targeted delivery of KHHR NCs into cancer cells. The expression level of

CD44 on cell surfaces was first evaluated by CD44 antibody staining and flow cytometry analysis, and all tested cancer cells (HeLa, B16F10, 4T1) showed notably higher CD44 expression levels than normal cells (3T1, L929, Figure S7, Supporting Information), which provided basis for HA-mediated cancer cell targeting. Confocal laser scanning microscopy (CLSM) observation showed that free FITC-RNBC was unappreciably taken up by HeLa cells due to its high MW and hydrophilicity (**Figure 2**A). Comparatively, when encapsulated in KHHR NCs, FITC-RNBC was notably internalized, as evidenced by the cytoplasmic distribution of green fluorescence. Separation of green fluorescence (FITC-RNBC) from red fluorescence (Lysotracker Red-stained endolysosomes) was clearly noted, indicating that the NCs were able to escape from endosomal entrapment as a result of KPEI-mediated "proton sponge" effect.[22] When cells were treated with KHHR NCs for 4 h and irradiated (635 nm, 5 mW cm^{-2}) for 30 min, cytoplasmic distribution as well as endosomal escape was similarly observed (Figure 2A), which demonstrated that light irradiation did not appreciably impact the intracellular delivery of RNBC. When cells were pre-treated with free HA to block the CD44 on cell surfaces, the uptake level of RNBC in HeLa cells was dramatically reduced (Figure 2A), further substantitating the HA-mediated cancer cell targeting via recognition of CD44. The cellular uptake level was further explored by flow cytometry and spectrofluorimetry (Figure 2B,C), and KHHR NCs consistently afforded notably higher cell uptake levels in all tested cancer cells (HeLa, B16F10, and 4T1) than in normal cells (3T3 and L929). Pretreatment with HA led to significant decrease of the cell uptake level in cancer cells but not in normal cells (Figure 2C), which collectively substantiated that the KHHR NCs delivered RNBC into cancer cells via CD44-mediated endocytosis.
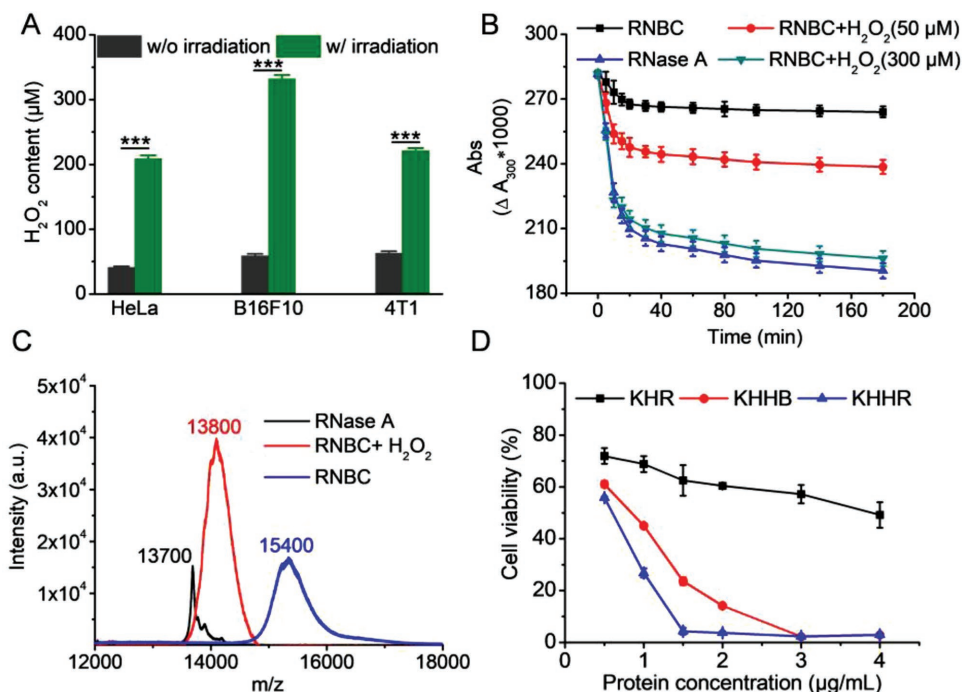
**ADVANCED
SCIENCE NEWS**
www.advancedsciencenews.com

**ADVANCED
FUNCTIONAL
MATERIALS**
www.afm-journal.de

Figure 3. Light irradiation enhanced intracellular H_2O_2 levels and restored the enzymatic activity of RNBC to achieve synergistic anti-tumor efficacy in vitro. A) H_2O_2 levels in various cancer cell lines following treatment with KHHR NCs for 4 h and light irradiation (635 nm, 5 mW cm^{-2}) for 30 min ($n = 3$). B) Hydrolysis of RNA by RNase A, RNBC, and H_2O_2-treated RNBC within the treatment period of 3 h ($n = 3$). $\Delta A_{300} = A_{300\ sample} - A_{300\ blank}$. C) MALDI-TOF spectra of RNase A, RNBC, and H_2O_2-treated RNBC. D) Cytotoxicity of KHR NCs, KHHB NCs, and KHHR NCs toward HeLa cells as determined by the MTT assay ($n = 3$). Cells were treated with NCs for 4 h, irradiated (635 nm, 5 mW cm^{-2}) for 30 min, and further incubated in fresh media for 20 h before the MTT assay.

2.4. In Vitro PDT-Enhanced ROS Generation and Restoration of Protein Activity

We next explored the light-induced H_2O_2 generation in cancer cells in vitro and evaluated whether the enhanced intracellular H_2O_2 production could promote the activation of RNBC to afford cancer-specific cytotoxicity. To this end, HeLa, B16F10, and 4T1 cells were incubated with KHHR NCs for 4 h and were irradiated (635 nm, 5 mW cm^{-2}) for 30 min before evaluation of intracellular ROS generation. 2′,7′-Dichlorofluorescein-diacetate (DCFH-DA) as a commonly used ROS probe can be oxidized by ROS to generate dichlorofluorescein (DCF) with green fluorescence.[23] As shown in Figure S8 (Supporting Information), HeLa cells treated with KHHR NCs showed stronger green fluorescence upon light irradiation, indicating remarkable production of ROS inside cells. In a further quantitative analysis using the Hydrogen Peroxide Assay Kit, we found that the cellular H_2O_2 concentration was enhanced by 4–6-fold (from 40–60 × 10^{-6} to 200–300 × 10^{-6} M) upon light irradiation (**Figure 3**A). In consistence with such H_2O_2 concentration enhancement, the enzymatic activity of RNBC was greatly recovered. Particularly, RNBC showed negligible capability to degrade RNA, and RNBC treated with 50 × 10^{-6} M H_2O_2 led to only 15% RNA hydrolysis, indicating that caging of the lysine residues in RNase A deprived its enzymatic activity and H_2O_2 treatment at the concentration ($\approx$50 × 10^{-6} M) in cancer cells only recovered a small proportion of its enzymatic activity (Figure 3B). Comparatively, at the enhanced H_2O_2 concentration (300 × 10^{-6} M) post light irradiation, the hydrolytic activity

against RNA was completely restored, leading to similar RNA degradation profiles to the native RNase A (Figure 3B). In support to such findings, the ARS fluorescence of H_2O_2-treated RNBC sharply decreased to that of RNase A (Figure S3, Supporting Information), and the MW of RNBC also restored to that of RNase A upon H_2O_2 treatment (Figure 3C). These results collectively substantiated that light irradiation of PS significantly enhanced the intracellular H_2O_2 level in cancer cells, which subsequently facilitated cleavage of the NBC caging groups on RNBC and converted the inactive RNBC back to the enzymatically active RNase A.

2.5. In Vitro Anti-Cancer Efficacy

The light-activated anti-cancer efficacy of RNBC and its synergistic effect with PS-mediated PDT were then explored in different cancer cell lines in vitro. Bovine serum albumin (BSA), instead of RNBC, was used to construct the KPEI/HA-Hp/BSA (KHHB) NCs to first evaluate the biocompatibility of the delivery vehicle. After incubation with HeLa cells for 24 h, the cell viability remained more than 90% at the BSA concentrations up to 10 μg mL^{-1} (Figure S9A, Supporting Information). Moreover, after incubation with H_2O_2-treated NBC for 24 h at the concentration up to 1 μg mL^{-1}, viability of HeLa cells remained higher than 90%, suggesting that the small molecules generated from the deprotection did not impart appreciable cytotoxicity (Figure S9B, Supporting Information). To explore the anti-cancer activity, KPEI/HA/RNBC

(KHR) NCs, KHHB NCs, and KHHR NCs were incubated with HeLa cells for 4 h followed by light irradiation (635 nm, 5 mW cm^{-2}) for 30 min. As shown in Figure 3D and Table S1 (Supporting Information), KHHR NCs displayed significantly stronger anti-cancer efficacy than KHR NCs (protein drug only) or KHHB NCs (PDT only), and the half-maximal inhibitory concentration (IC$_{50}$) of RNBC in KHHR NCs (0.58 µg mL^{-1}) was ≈6-fold lower than that in KHR NCs (3.87 µg mL^{-1}), which could be attributed to the restoration of the hydrolytic activity of RNBC upon Hp-mediated H$_2$O$_2$ generation. Similar results were also observed in B16F10 and 4T1 cells, where the IC$_{50}$ of RNBC or Hp in KHHR NCs was notably decreased compared to those in KHR NCs or KHHB NCs (Figure S10 and Table S1, Supporting Information). More importantly, the combination index (CI) between RNBC and Hp was calculated to be lower than 1 in all three cell lines (HeLa, B16F10, and 4T1), substantiating the synergistic effect between RNBC and Hp-mediated PDT (Table S1, Supporting Information). Pre-incubation of cells with free HA prior to the treatment with KHHR NCs led to enhanced IC$_{50}$ of RNBC (Table S2, Supporting Information), which was consistent with our previous findings on HA-mediated cancer cell targeting.

2.6. Tumor Accumulation and In Vivo Cellular Uptake

Prior to the in vivo efficacy study, the blood circulation half-life and biodistribution of KHHR NCs containing Cy5.5-RNBC were monitored following i.v. injection (1.75 mg Cy5.5-RNBC kg^{-1}) to normal mice or 4T1 tumor-bearing mice. Compared to free RNBC and KR NCs that were rapidly cleared from the blood within 5 h (half-life ≈0.40 and 0.39 h, respectively), plasma RNBC could still be detected at 24 h post-injection of KHHR NCs (half-life ≈3.20 h, **Figure 4**D). Such prolonged circulation time of KHHR NCs could be ascribed to the HA coating on NCs that shielded the positive charges on KPEI to endow the NCs with enhanced stability in serum and reduced clearance by the RES. As a result of the "long circulation" property, KHHR NCs were allowed to accumulate in tumor tissues via the enhanced EPR effect. As shown by the in vivo fluorescence imaging (Figure 4A,B), mice injected with KHHR NCs showed notably stronger fluorescence in tumors than those injected with free RNBC at 6 h post-injection. The Cy5.5-RNBC fluorescence of KHHR NCs remained strong in tumors even at 24 h post-injection while negligible fluorescence could be observed for the free Cy5.5-RNBC (Figure 4A), which further demonstrated that KHHR NCs afforded high tumor accumulation and
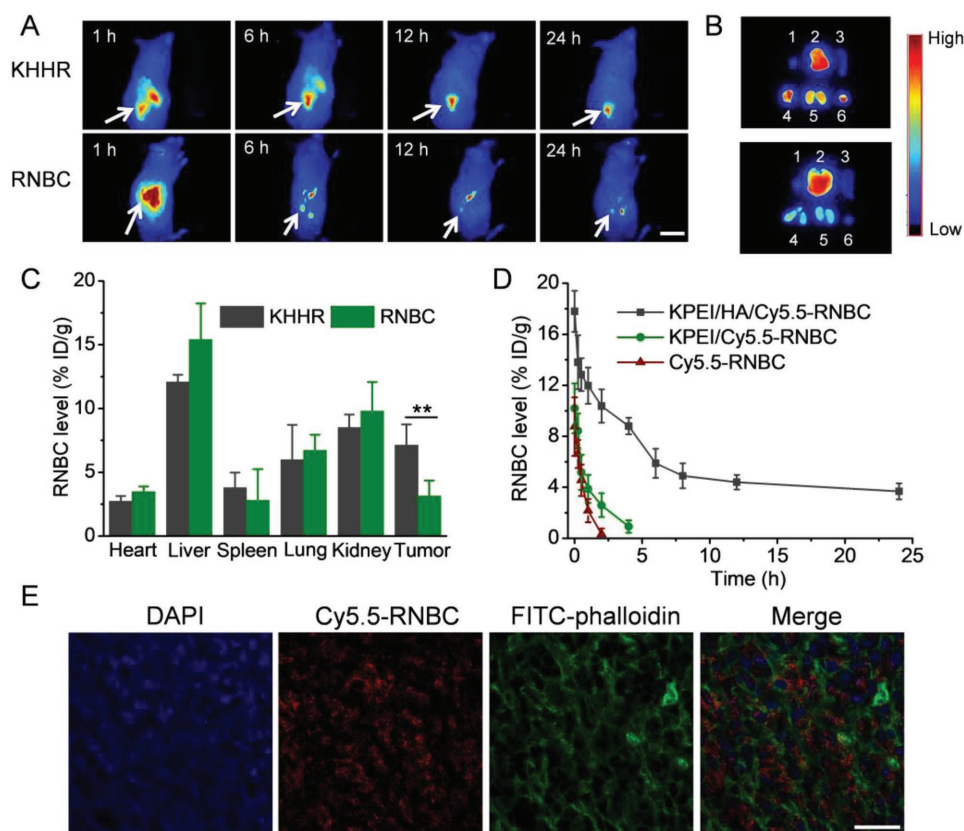

Figure 4. Tumor accumulation and cancer cell uptake of KHHR NCs in vivo. A) In vivo fluorescence imaging of 4T1 mammary tumor-bearing mice at 1, 6, 12, and 24 h post i.v. injection of free Cy5.5-RNBC or KHHR NCs containing Cy5.5-RNBC. Arrows refer to the tumors. Bar represents 20 mm. B) Ex vivo fluorescence imaging of excised tumors and major organs at 6 h post i.v. injection (1: heart; 2: liver; 3: spleen; 4: lung; 5: kidney; 6: tumor). C) Biodistribution levels of Cy5.5-RNBC in tumors and major organs at 6 h post i.v. injection ($n = 3$). D) Pharmacokinetics of KHHR NCs, KR NCs, and RNBC following i.v. injection ($n = 3$). E) CLSM images of tumor sections excised from mice at 6 h post i.v. injection of KHHR NCs containing Cy5.5-RNBC. The cell nuclei and cell membranes were stained with DAPI (blue) and FITC-phalloidin (green), respectively. Bar represents 100 µm.

retention. In a quantitative analysis on the biodistribution level, the tumor tissues and major organs were harvested and lysed at 6 h post-injection, and the Cy5.5-RNBC level in the supernatant was quantified by spectrofluorimetry. Consistent results were obtained, wherein the tumor accumulation level of Cy5.5-RNBC was 7.1% ID g^{-1} for KHHR NCs, 2.3-fold higher than free Cy5.5-RNBC (Figure 4C). With the attempt to evaluate the delivery of RNBC into cancer cells in vivo, 4T1 xenograft tumors were harvested, cryo-sectioned, and observed by CLSM following staining with DAPI and FITC-phalloidin. Extensive intracellular distribution of red fluorescence (Cy5.5-RNBC) was noted (Figure 4E), which confirmed that KHHR NCs successfully delivered the RNBC into cancer cells after accumulating in tumor tissues.

2.7. In Vivo Anti-Cancer Efficacy

The in vivo anti-cancer efficacy was then evaluated in 4T1 xenograft tumor-bearing mice. NCs were i.v. injected on day 1 and 4 (Hp, 10 mg kg^{-1}; RNBC, 1.75 mg kg^{-1}), and tumors were irradiated (635 nm, 5 mW cm^{-2}) for 30 min at 12 h post-injection

(**Figure 5**A). Within the 12 d observation period, tumor growth was partly inhibited for the KHHB NCs (PDT only) and KHR NCs (protein drug only), while tumors treated with KHHR NCs almost stopped growing (Figure 5B and Figure S11, Supporting Information), which indicated the synergistic antitumor efficacy enabled by the combination of light-mediated PDT and PDT-activated protein therapy. PBS-treated mice began to lose weight on day 8, indicating that the living quality of mice was compromised by the tumor burden. Comparatively, the body weight of mice receiving different NCs gradually increased (Figure S12, Supporting Information), indicating the minimal systemic toxicity of NCs. Such result was further supported by the minimal pathological abnormalities of major organs following H&E staining (Figure S13, Supporting Information). At 12 h post the second injection of KHHR NCs (same administration protocol as in the efficacy study), serum alanine amino transferase (ALT) and aspartate amino transferase (AST) levels were unappreciably increased (Figure S14, Supporting Information), indicating minimal toxicity of KHHR NCs to liver tissues. In consistence with the tumor volume progression, the histologic images of the H&E-stained tumor sections showed the highest cancer cell remission after treatment with KHHR NCs
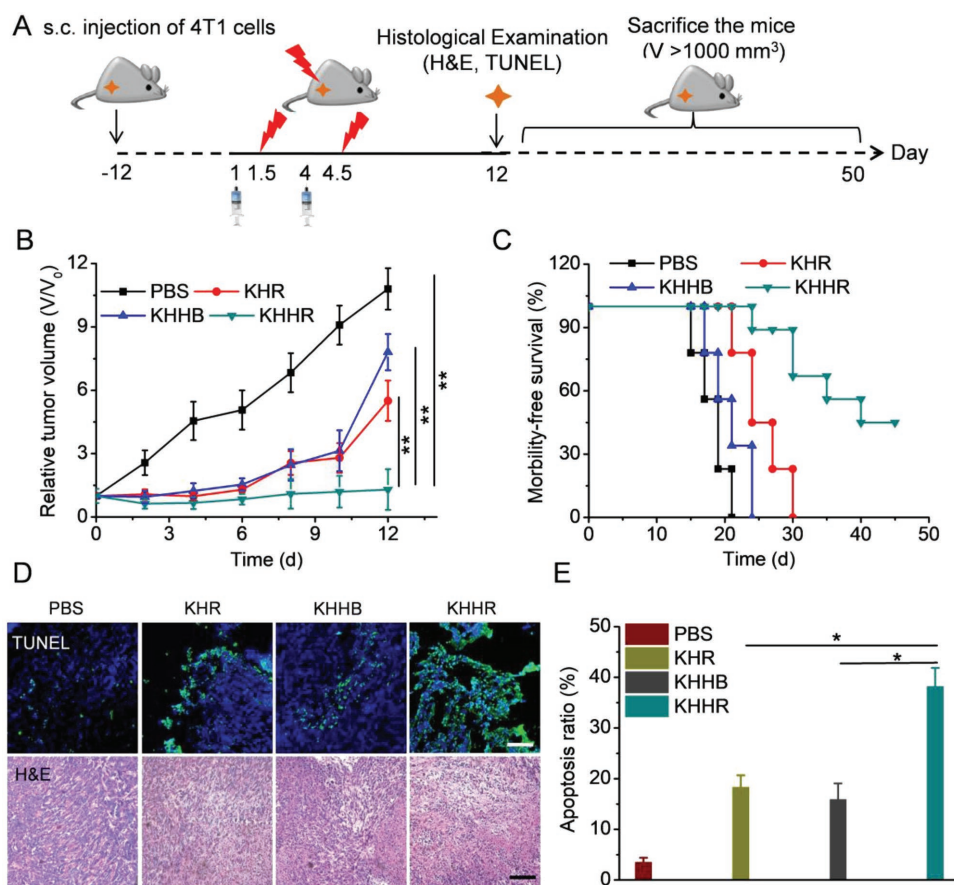

Figure 5. Light-enhanced synergistic anti-cancer efficacy of KHHR NCs in 4T1 mammary tumor-bearing mice. A) Schematic illustration showing the time line of the efficacy study. B) Tumor volume change of mice receiving i.v. injections of PBS, KHR NCs, KHHB NCs, and KHHR NCs on days 1 and 4 (Hp, 10 mg kg^{-1}; RNBC, 1.75 mg kg^{-1}) (n = 9). Mice were irradiated (635 nm, 5 mW cm^{-2}) for 30 min at 12 h post-injection. C) Survival rate of mice treated as described in (A) within the observation period of 46 d (n = 9). D) TUNEL and H&E staining of tumor sections excised from mice on day 12 following the treatment as described in (A). Bar represents 100 μm. E) Apoptosis ratio of tumor cells as determined by the TUNEL assay in (D) using the ImageJ software (n = 3, 8 random microscope fields for each tumor slice).

**ADVANCED
SCIENCE NEWS**
www.advancedsciencenews.com

**ADVANCED
FUNCTIONAL
MATERIALS**
www.afm-journal.de

(Figure 5D), and the in situ TUNEL assay revealed the highest apoptosis level in the tumors collected from mice treated with KHHR NCs (Figure 5D,E). As a conquence, animals administered with KHHR NCs showed the highest survival rate (45%) within the observation period of 46 d (Figure 5C).

3. Conclusions

In summary, we constructed a unique "all-functions-in-one" nanovehicle coupled with photoresponsive, reversible protein engineering to realize the effective and selective delivery of protein drugs toward cancer treatment. The nanovehicle possessed synchronized functionalities of stable protein encapsulation, high serum stability, long blood circulation, cancer cell targeting, endosomal escape, and trigger-responsive intracellular drug release, which collectively circumvented the various systemic barriers against anti-cancer protein delivery. A ROS-cleavable, reversibly caged protein prodrug was engineered, which can restore activity upon PS-mediated ROS generation under long-wavelength visible light (635 nm) irradiation at low power density (5 mW cm^{-2}), thereby improving the selectivity of the protein drug in killing cancer cells. Potent anti-cancer efficacy was thus achieved upon a synergistic combination of PS-mediated PDT and protein-mediated chemotherapy. To the best of our knowledge, no other nanoparticle-based delivery vehicle has been reported so far that possesses all of the above synchronized attributes, which makes it the first example of a nanocarrier that simultaneously addresses the material requirements for mediating efficient and targeted protein delivery into cancer cells. It is also the first time to realize the photo-manipulation of protein functions by coupling ROS-cleavable protein caging with PS-mediated ROS generation in response to long-wavelength light irradiation at low power density. This study therefore provides a universal platform for programmed anti-cancer protein therapy, and it would find broad utilities for light-controlled delivery of other cargo molecules, such as genes and chemo-drugs.

4. Experimental Section

Materials, Cells, and Animals: Pinacol, phenylboronic acid, and haematoporphyrin were purchased from Alfa Aesar (Shanghai, China). 4-Nitrophenyl chloroformate was purchased from Energy Chemical (Shanghai, China). HA (MW = 35 kDa) was purchased from Shandong Freda Biopharm Co. Ltd. (Jinan, China). ARS and branched polyethylenimine (PEI, MW = 600 Da) were purchased from J&K (Beijing, China). Bovine pancreatic ribonuclease A (RNase A), BSA, and phalloidin were purchased from Sigma-Aldrich (St. Louis, MO). Fluorescein isothiocyanate (FITC) and 3-(4,5-dimethylthiahiazol-2-yl)-2,5-diphenyl-2*H*-tetrazolium bromide (MTT) were purchased from Invitrogen (Carlsbad, CA). Cy5.5-NHS was purchased from Lumiprobe (Maryland, USA). All solvents were purchased from Sinopharm Chemical Reagent Co. Ltd. (Shanghai, China).

HeLa (human cervix adenocarcinoma), B16F10 (mouse melanoma), 4T1 (mouse mammary carcinoma), 3T3 (mouse embryonic fibroblast), and L929 (mouse fibroblast) cells were purchased from the American Type Culture Collection (Rockville, MD). HeLa, 3T3, and L929 cells were cultured in Dulbecco's modified Eagle medium (DMEM) (Gibco, Grand Island, NY) containing 10% fetal bovine serum (FBS). B16F10 and 4T1 cells were cultured in RPMI-1640 (Gibco, Grand Island, NY) containing 10% fetal bovine serum.

Female BALB/c mice (6–8 weeks) were purchased from Shanghai Slaccas Experimental Animal Co. Ltd. (Shanghai, China) and housed in a clean room, five to a cage, with access to water ad libitum, a 12:12 h light–dark cycle (7:00–19:00), and a temperature of 25 ± 1 °C. All animal study protocols were reviewed and approved by the Institutional Animal Care and Use Committee, Soochow University.

Synthesis and Characterization of KPEI: The ketal cross-linker, *n*-{2-[1-(2-acryloylamino-ethoxy)-1-methylethoxy]-ethyl}-acrylamide (AEA), was synthesized according to a previous report (Scheme S1A, Supporting Information).[24] KPEI was synthesized via the Michael addition between AEA and PEI 600 Da (Scheme S1B, Supporting Information). Briefly, PEI 600 Da (50 mg) was dissolved in methyl alcohol (1 mL) and heated to 45 °C in a two-necked flask under the nitrogen atmosphere. AEA (34 mg, molar ratio of acrylate in AEA to primary amine in PEI = 1:2) was dissolved in methyl alcohol (1 mL) and added to the PEI solution. The mixture was stirred in the dark for 48 h. The obtained KPEI polymer was dialyzed against distilled (DI) water (pH = 8, MWCO = 1 kDa) for 3 d and lyophilized. The MW of the polymer was measured by MALDI-TOF (Bruker, ultraflextreme MALDI-TOF/TOF).

Synthesis of RNBC and Fluorescence-Labeled RNBC: **Compound 1** was synthesized as described previously with slight modification (Scheme S2, Supporting Information).[25] Pinacol (0.79 g, 1 equiv) and phenylboronic acid (1 g, 1 equiv) were added to anhydrous THF (40 mL), and the mixture was refluxed overnight. After being cooled to RT, the solvent was removed by rotary evaporation, and the residue was dissolved in dichloromethane (DCM, 100 mL) and washed with water (70 mL × 3). The organic phase was combined and dried over anhydrous MgSO$_4$. Finally, the solution was filtered and concentrated by rotary evaporation to obtain the residue which was further purified by silica gel column chromatography using DCM/ethyl acetate (9/1, v/v) as the eluent to obtain **compound 1** as white powder (1.27 g, 82.2% yield).

Compound 2, NBC, was synthesized as described previously.[26] Briefly, **compound 1** (0.5 g, 1 equiv) was dissolved in anhydrous THF (20 mL) into which 4-nitrophenyl chloroformate (0.47 g, 1.1 equiv) and TEA (0.6 ml, 2 equiv) were added. After stirring at RT for 1 h, the solvent was removed by rotary evaporation, and the residue was dissolved in ethyl acetate (100 mL) and washed with water (70 mL × 3), HCl solution (1 M, 70 mL × 3), and NaHCO$_3$ solution (70 mL × 3). The organic phase was combined and dried over anhydrous MgSO$_4$. The solution was filtered and concentrated by rotary evaporation to obtain the residue which was further purified by silica gel column chromatography using petroleum ether/ethyl acetate (5/1, v/v) as the eluent to obtain **compound 2** as white powder (0.56 g, 66.7% yield).

RNase A was then modified via caging of the primary amine groups on the lysine residues with NBC. Briefly, RNase A (3 mg) and NBC (9.6 mg) were separately dissolved in NaHCO$_3$ solution (0.1 M, pH 8.5) and DMSO which were mixed and stirred at RT for 10 h. The mixture was then purified by ultrafiltration (MWCO = 3 kDa) and lyophilized to obtain RNBC as white powder. The fluorometric ARS assay was performed to confirm conjugation of phenylboronic acid moieties to RNase A. Briefly, RNBC was dissolved in DI water (0.25 mg mL^{-1}) and treated with H$_2$O$_2$ (final concentration of 300 × 10^{-6} M) at 37 °C for 3 h. H$_2$O$_2$-treated RNBC and nontreated RNBC were separately added to the ARS solution (0.025‰, w/v), and the mixture was incubated at 37 °C for 15 min followed by the measurement of fluorescence intensity (λ_{ex} = 490 nm, λ_{em} = 600 nm).

To allow the observation and quantification of RNBC in vitro and in vivo, RNBC was labeled with fluorescent tags. For in vitro use, RNBC (2 mg) was dissolved in NaHCO$_3$ solution (0.1 M, pH 9.5), and the FITC solution (4 mg mL^{-1} in DMSO, 250 µL) was added to the RNBC solution which was stirred in the dark at RT for 2 h. The obtained FITC-RNBC was purified by ultrafiltration (MWCO = 3 kDa) against DI water and lyophilized. For in vivo use, Cy5.5-RNBC was synthesized similarly. RNBC (5 mg) was dissolved in NaHCO$_3$ solution (0.1 M, pH = 9.5), and the Cy5.5-NHS solution (4 mg mL^{-1} in DMSO, 250 µL) was added to the RNBC solution which was stirred in the dark at RT overnight. The

obtained Cy5.5-RNBC was purified by ultrafiltration (MWCO = 3 kDa) against DI water (pH = 9.5) and lyophilized.

Synthesis of HA-Haematoporphyrin: HA (38 mg, 1 equiv of carboxyl group) was dissolved in NaHCO$_3$ solution (0.1 M, pH 8.5), into which EDC (18.7 mg, 2 equiv) and DMAP (14.7 mg, 2.5 equiv) were added. After stirring at RT overnight, Hp (36 mg, 1 equiv) was added and the reaction mixture was further stirred in the dark for 48 h. The obtained HA-Hp was dialyzed against DI water (MWCO = 3 kDa) for 2 d and lyophilized. The Hp content was determined to be 385 μg mg^{-1} HA as measured by the UV–vis method.[27]

H_2O_2-Triggered Re-activation of RNBC: To demonstrate the H$_2$O$_2$-induced cleavage of phenylboronic acid moieties, RNBC was dissolved in DI water at 10 mg mL^{-1} and treated with H$_2$O$_2$ at various final concentrations (50 and 300 × 10^{-6} M) for 3 h. The MW of RNBC before and after H$_2$O$_2$ treatment was determined by MALDI-TOF. The H$_2$O$_2$-treated RNBC as described above was also subjected to the assessment of enzymatic activity using a Ribonuclease A Detection Kit (Sigma-Aldrich, USA) to explore the H$_2$O$_2$-mediated recovery of hydrolytic activity of RNase A.

Preparation and Characterization of NCs: KPEI, HA-Hp, and RNBC were separately dissolved in DI water at 1 mg mL^{-1}. HA-Hp was added to RNBC at the HA-Hp/RNBC weight ratio of 15/1, and the mixture was vortexed for 10 s and incubated at 37 °C for 10 min. KPEI was then added to the mixture at the KPEI/RNBC weight ratio of 15/1, which was further incubated at RT for 1 h to allow formation of the KPEI/HA-Hp/RNBC (KHHR, K represents KPEI, HH represents HA-Hp, R represents RNBC) NCs. The component and the acronym of different NCs are summarized in Table S3 (Supporting Information). The particle size and zeta potential were monitored by DLS on a Malvern Zetasizer. The KHR and KHHB NCs were prepared following the same method as described above. To evaluate the DLC and DLE of RNBC in KHHR NCs, the freshly prepared KHHR NCs containing FITC-RNBC were purified via ultrafiltration to remove free FITC-RNBC, and they were lyophilized and dissolved in DMF. The RNBC concentration was quantified by spectrofluorimetry (λ_{ex} = 490 nm, λ_{em} = 525 nm) to calculate the DLC and DLE.

To evaluate the stability of NCs, freshly prepared KHHR NCs were diluted with DMEM containing 10% serum for tenfold and incubated at RT for different time before measurement of particle size. To further evaluate the stability of NCs in the slightly acidic environment in tumor tissues, KHHR NCs were diluted with PBS buffer (pH 6.8) before measurement of size alteration as described above.

FITC-RNBC release from KHHR NCs was studied at pH 5.0 and 7.4 using the dialysis method. Briefly, freshly prepared NCs (200 μL) containing FITC-RNBC were placed inside the dialysis bag (MWCO = 35 kDa) which was incubated in PBS (pH 7.4, 150 × 10^{-3} M, 30 mL) or acetate buffer (pH 5.0, 150 × 10^{-3} M, 30 mL) at 37 °C and 200 rpm. At predetermined time intervals, the release medium (1 mL) was collected and the RNBC concentration was quantified by spectrofluorimetry (λ_{ex} = 490 nm, λ_{em} = 525 nm) to calculate the accumulative drug release amount. The release medium was refreshed with 1 mL of fresh medium to maintain a constant volume.

Determination of Intracellular H_2O_2 Level: For the qualitative observation of ROS generation in cells, HeLa cells before and after light irradiation were assayed by using the Reactive Oxygen Species Assay Kit (Beyotime Biotechnology, China). Briefly, HeLa cells were seeded on 24-well plates at 3 × 10^4 cells/well and cultured for 24 h. The medium was changed to opti-MEM and KHHR NCs were added at the RNBC concentration of 6 μg mL^{-1}. After incubation at 37 °C for 4 h, cells were washed three times with PBS, incubated with DCFH-DA (10 × 10^{-6} M), irradiated by 635 nm light (Maestro, In-vivo Imaging System) at the power density of 5 mW cm^{-2} for 30 min, fixed with paraformaldehyde (4%), and stained with DAPI (5 μg mL^{-1}) before CLSM observation.

To quantify the generation of H$_2$O$_2$ in cells before and after light irradiation, HeLa cells were seeded on 96-well plates at 2 × 10^4 cells/well and cultured for 24 h. The medium was changed to opti-MEM (90 μL well^{-1}) and KHHR NCs were added at the RNBC concentration of 3 μg mL^{-1}. After incubation at 37 °C for 4 h, the medium was replaced by fresh DMEM containing 10% FBS. Cells were then irradiated by 635 nm light (Maestro, In-vivo Imaging System) at the power density of 5 mW cm^{-2} for 30 min, lysed with the assay buffer, and subjected to measurement of H$_2$O$_2$ content in the cell lysate using the Hydrogen Peroxide Assay Kit (Beyotime Biotechnology, China) according to the manufacturer's protocol. Non-irradiated cells served as the control. The generality of light-mediated H$_2$O$_2$ generation was also evaluated in B16F10 and 4T1 cells using the same method.

Intracellular Kinetics: To measure the CD44 expression levels on cell surfaces, HeLa cells were seeded on coverslips in 24-well plate at 1 × 10^5 cells/well and were cultured for 24 h. Cells were then incubated with the CD44 PE antibody (eBioscience, 1:50) at 37 °C for 1 h, washed three times with PBS, and digested by trypsin without EDTA. The suspension was centrifuged at 1000 × g for 5 min, washed twice with PBS, and resuspended with 300 μL PBS. Fluorescence histograms were then recorded with a BD FACSCalibur flow cytometer (Beckton Dickinson, USA) and analyzed using the Cell Quest software. The CD44 expression levels were also monitored in B16F10, 4T1, 3T3, and L929 cells using the same method.

To evaluate the cellular uptake of KHHR NCs, HeLa cells were seeded on 24-well plates at 1 × 10^5 cells/well and were cultured for 24 h. The medium was changed to opti-MEM, into which FITC-RNBC and KHHR NCs containing FITC-RNBC were added at the FITC-RNBC concentration of 6 μg mL^{-1}. After incubation at 37 °C for 4 h, cells were washed three times with PBS and digested by trypsin without EDTA. The suspensions were centrifuged at 1000 × g for 5 min, washed twice with PBS, and resuspended with 300 μL PBS. The uptake level was explored by flow cytometry (Beckton Dickinson, USA) and the data were analyzed using the Cell Quest software. To further probe the HA-assisted targeting effect, cells were pretreated with free HA (final concentration of 10 mg mL^{-1}) for 4 h and washed three times with PBS before KHHR NCs were added.

The internalization and intracellular distribution of KHHR NCs containing FITC-RNBC were also visualized by CLSM. Briefly, HeLa cells were seeded on coverslips in 24-well plate at 3 × 10^4 cells/well and were incubated for 24 h before treatment with KHHR NCs in opti-MEM at the FITC-RNBC concentration of 6 μg mL^{-1} for 4 h. Cells were washed three times with PBS, stained with Lysotracker Red (200 × 10^{-9} M), fixed with paraformaldehyde (4%), and stained with DAPI (5 μg mL^{-1}) before CLSM observation. To evaluate the effect of light irradiation on cellular kinetics, cells treated with KHHR NCs for 4 h were irradiated (635 nm, 5 mW cm^{-2}) for 30 min, further incubated for 4 h, stained as described above, and visualized by CLSM. To probe the HA-assisted targeting effect, cells were pretreated with free HA (final concentration of 10 mg mL^{-1}) for 4 h and washed three times with PBS before KHHR NCs were added.

To quantify the cellular uptake level of RNBC, HeLa cells were seeded on 96-well plates at 1 × 10^4 cells/well and cultured for 24 h. The medium was changed to opti-MEM, into which KHHR NCs containing FITC-RNBC were added at the FITC-RNBC concentration of 10 μg mL^{-1}. After incubation at 37 °C for 4 h, cells were washed three times with PBS and lysed with the RIPA lysis buffer. FITC-RNBC content in the lysate was measured by spectrofluorimetry (λ_{ex} = 490 nm, λ_{em} = 525 nm) and the protein content was measured by using the BCA kit (Pierce). Uptake level was expressed as ng FITC-RNBC associated with 1 mg cellular protein. The cellular uptake levels of RNBC in B16F10, 4T1, 3T3, and L929 cells were monitored using the same method. To study the HA-assisted targeting effect of NCs, cells were pretreated with free HA (final concentration of 10 mg mL^{-1}) for 4 h before addition of KHHR NCs. The uptake level of FITC-RNBC was measured 4 h later as described above.

In Vitro Anticancer Efficacy: The cytotoxicity of the nanocarrier was first evaluated. Briefly, HeLa cells were seeded on 96-well plates at 1 × 10^4 cells/well and cultured for 24 h. KHHB NCs were separately added at various BSA final concentrations, and cells were incubated for 24 h before viability assessment by the MTT assay. To evaluate the toxicity of generated small molecules after deprotection of NBC moieties, NBC was treated with H$_2$O$_2$ (300 × 10^{-6} M, 3 h), deactivated with peroxidase,

ADVANCED
SCIENCE NEWS
www.advancedsciencenews.com

ADVANCED
FUNCTIONAL
MATERIALS
www.afm-journal.de

and incubated with HeLa cells at various final concentrations for 24 h before viability test using the same method.

To further study the in vitro anticancer efficacy, KHR NCs (deprived of the PS), KHHB NCs (RNBC replaced by BSA), and KHHR NCs were incubated with HeLa cells in 96-well plates at various final concentrations of RNBC or BSA at 37 °C for 4 h. The NCs were then removed, and the medium was replaced by fresh DMEM containing 10% FBS. Cells were irradiated by 635 nm light (Maestro, In-vivo Imaging System) at the power density of 5 mW cm^{-2} for 30 min, and further incubated for another 20 h before viability assessment by the MTT assay. The in vitro anticancer efficacy was also explored in B16F10 and 4T1 cells using the same method. The IC$_{50}$ (half inhibitory concentration) value of RNBC or Hp was calculated. To further investigate the synergistic effect between RNBC and Hp-mediated photodynamic therapy, the CI was calculated according to Chou and Talalay's method[28] as follows

$$CI = \frac{D_1}{D_{m1}} + \frac{D_2}{D_{m2}} \tag{1}$$

where D_1 and D_2 denote the IC$_{50}$ of drug 1 (RNBC) and drug 2 (Hp) in the combination system (KHHR NCs). D_{m1} and D_{m2} denote the IC$_{50}$ of drug 1 (RNBC in KHR NCs) and drug 2 (PS in KHHB NCs) alone, respectively. The CI values lower than, equal to, and higher than 1 denote synergism, additivity, and antagonism, respectively.

To further probe the HA-assisted targeting effect, CD44$^+$ cells expressing HA receptors (B16F10 and 4T1) were pretreated with free HA (final concentration of 10 mg mL^{-1}) for 4 h, washed with PBS for three times, and treated with NCs as described above before the MTT assay.

Pharmacokinetics and Biodistribution: For the pharmacokinetics study, female BALB/c mice were divided into three groups ($n = 3$), which, respectively, received i.v. injection of KHHR NCs, KR NCs, and free Cy5.5-RNBC at 1.75 mg RNBC kg^{-1}. Blood (20 μL) was collected from the orbit at different time points post-injection, and was dissolved in lysis buffer (1% Triton X-100, 100 μL) with sonication. Cy5.5-RNBC was extracted by incubation of the blood samples in HCl-IPA at −20 °C overnight. After centrifugation at 12 000 rpm for 30 min, Cy5.5-RNBC level in the supernatant was determined by spectrofluorimetry ($\lambda_{ex} = 684$ nm, $\lambda_{em} = 710$ nm).

For the biodistribution study, female BALB/c mice were unhaired, anesthetized by isoflurane, and subcutaneously injected with 1×10^7 4T1 cells in the right flank. When the tumor volume reached 150 mm^3, mice were divided into two groups ($n = 3$). The first group received i.v. injection of KHHR NCs (1.75 mg RNBC kg^{-1}) while the second group received i.v. injection of free Cy5.5-RNBC (1.75 mg RNBC kg^{-1}). Fluorescence imaging was performed at various time points post i.v. injection using the In-Vivo Imaging System (Maestro). In a parallel study, at 6 h post i.v. injection, mice were sacrificed. The tumor tissues and major organs including heart, liver, spleen, lung, and kidney were collected and washed with PBS. Fluorescence imaging of these tissues was acquired using the In-Vivo Imaging System (Maestro). To further quantify the Cy5.5-RNBC levels in tumor and major organs, these tissues were harvested at 6 h post i.v. injection, washed with PBS, weighed, and homogenized with 1% Triton X-100. Cy5.5-RNBC was extracted by incubation of the homogenate with HCl-IPA at −20 °C overnight. After centrifugation at 12 000 rpm for 30 min, Cy5.5-RNBC level in the supernatant was determined by spectrofluorimetry ($\lambda_{ex} = 684$ nm, $\lambda_{em} = 710$ nm).

To further explore the in vivo uptake of RNBC in cancer cells, 4T1 tumor-bearing mice were i.v. injected with KHHR NCs containing Cy5.5-RNBC, and animals were sacrificed at 6 h post-injection. The tumors were collected, washed with PBS, embedded in the OCT compound, sectioned, and stained with DAPI (5 μg mL^{-1}) and FITC-phalloidin (50 μg mL^{-1}, Sigma, USA) before observation with CLSM.

In Vivo Anticancer Efficacy: Female BALB/c mice were unhaired, anesthetized by isoflurane, and subcutaneously injected with 1×10^7 4T1 cells in the right flank. When the tumor volume reached 50 mm^3, mice were divided into four groups ($n = 9$). Mice in each group were i.v. injected with PBS or NCs (10 mg Hp kg^{-1}; 1.75 mg RNBC kg^{-1}) on

day 1 and 4. Group 1 received i.v. injection of PBS. Group 2 received i.v. injection of KHR NCs. Group 3 was i.v. injected with KHHB NCs and light irradiated (635 nm, 5 mW cm^{-2}) for 30 min at 12 h post-injection. Group 4 was i.v. injected with KHHR NCs and light irradiated (635 nm, 5 mW cm^{-2}) for 30 min at 12 h post-injection. The antitumor efficacy was assessed by measuring the tumor volume, body weight, and survival rate of mice in each group every other day. Tumor volume (V) was calculated as length × (width)^2 × 0.5. Relative tumor volume was calculated as V/V_0 (V_0 represents the tumor volume before treatment). Mice were considered to be dead either when the tumor volume reached 1000 mm^3 or when the mice died during the treatment. To evaluate the liver toxicity, blood was collected at 12 h post the second injection, and serum ALT/AST levels were measured.

Histological Examination: Mice bearing 4T1 xenograft tumors received the same treatment as described above in the efficacy study. On day 12, tumors and major organs were harvested, fixed with 4% formalin, and embedded in paraffin. The sliced organs were stained with haematoxylin and eosin (H&E) and examined under a microscope. To further observe the apoptotic level of tumor cells, the harvested tumors were embedded in OCT and the frozen tissues were sectioned, stained with DAPI (5 μg mL^{-1}), and assayed using the One Step TUNEL Apoptosis Assay Kit (Beyotime Biotechnology, China) according to the manufacturer's protocol. All cells were stained with blue fluorescence (DAPI), and apoptotic cells showed green fluorescence. The apoptosis ratio was calculated as the percentage of apoptotic cells.

Statistical Analysis: Statistical analysis was performed using Student's *t*-test. The differences between test and control groups were judged to be significant at *$p < 0.05$ and very significant at **$p < 0.01$, ***$p < 0.001$.

Supporting Information

Supporting Information is available from the Wiley Online Library or from the author.

Conflict of Interest

The authors declare no conflict of interest.

[1] a) B. Leader, Q. J. Baca, D. E. Golan, *Nat. Rev. Drug Discovery* **2008**, *7*, 21; b) G. Walsh, *Nat. Biotechnol.* **2014**, *32*, 992; c) M. J. Hawkins, P. Soon-Shiong, N. Desai, *Adv. Drug Delivery Rev.* **2008**, *60*,

876; d) Y. Yang, Y. Niu, J. Zhang, A. K. Meka, H. Zhang, C. Xu, C. X. C. Lin, M. Yu, C. Yu, *Small* **2015**, *11*, 2743; e) K. Dutta, D. Hu, B. Zhao, A. E. Ribbe, J. Zhuang, S. Thayumanavan, *J. Am. Chem. Soc.* **2017**, *139*, 5676.

[2] a) J. A. Zuris, D. B. Thompson, Y. Shu, J. P. Guilinger, J. L. Bessen, J. H. Hu, M. L. Maeder, J. K. Joung, Z.-Y. Chen, D. R. Liu, *Nat. Biotechnol.* **2015**, *33*, 73; b) V. Postupalenko, D. Desplancq, I. Orlov, Y. Arntz, D. Spehner, Y. Mely, B. P. Klaholz, P. Schultz, E. Weiss, G. Zuber, *Angew. Chem., Int. Ed.* **2015**, *54*, 10583; c) H. Chang, J. Lv, X. Gao, X. Wang, H. Wang, H. Chen, X. He, L. Li, Y. Cheng, *Nano Lett.* **2017**, *17*, 1678; d) M. Yu, J. Wu, J. Shi, O. C. Farokhzad, *J. Controlled Release* **2016**, *240*, 24.

[3] S. Mitragotri, P. A. Burke, R. Langer, *Nat. Rev. Drug Discovery* **2014**, *13*, 655.

[4] a) M. Yan, J. Du, Z. Gu, M. Liang, Y. Hu, W. Zhang, S. Priceman, L. Wu, Z. H. Zhou, Z. Liu, T. Segura, Y. Tang, Y. Lu, *Nat. Nanotechnol.* **2010**, *5*, 48; b) B. Esteban-Fernandez de Avila, D. E. Ramirez-Herrera, S. Campuzano, P. Angsantikul, L. Zhang, J. Wang, *ACS Nano* **2017**, *11*, 5367; c) W.-J. Kim, B.-S. Kim, Y.-D. Cho, W.-J. Yoon, J.-H. Baek, K.-M. Woo, H.-M. Ryoo, *Biomaterials* **2017**, *122*, 154.

[5] a) J. E. Dixon, G. Osman, G. E. Morris, H. Markides, M. Rotherham, Z. Bayoussef, A. J. El Haj, C. Denning, K. M. Shakesheff, *Proc. Natl. Acad. Sci. USA* **2016**, *113*, 291; b) V. Torchilin, *Drug Discovery Today* **2008**, *5*, 95.

[6] a) Z. Gu, A. Biswas, M. Zhao, Y. Tang, *Chem. Soc. Rev.* **2011**, *40*, 3638; b) Y. Lu, W. Sun, Z. Gu, *J. Controlled Release* **2014**, *194*, 1; c) M. Wang, J. A. Zuris, F. Meng, H. Rees, S. Sun, P. Deng, Y. Han, X. Gao, D. Pouli, Q. Wu, I. Georgakoudi, D. R. Liu, Q. Xu, *Proc. Natl. Acad. Sci. USA* **2016**, *113*, 2868; d) M. C. Morris, J. Depollier, J. Mery, F. Heitz, G. Divita, *Nat. Biotechnol.* **2001**, *19*, 1173; e) J. E. Chung, S. Tan, S. J. Gao, N. Yongvongsoontorn, S. H. Kim, J. H. Lee, H. S. Choi, H. Yano, L. Zhuo, M. Kurisawa, J. Y. Ying, *Nat. Nanotechnol.* **2014**, *9*, 907; f) Y. Zhang, H. F. Chan, K. W. Leong, *Adv. Drug Delivery Rev.* **2013**, *65*, 104; g) R. H. Fang, C.-M. J. Hu, B. T. Luk, W. Gao, J. A. Copp, Y. Tai, D. E. O'Connor, L. Zhang, *Nano Lett.* **2014**, *14*, 2181; h) N. Yim, S.-W. Ryu, K. Choi, K. R. Lee, S. Lee, H. Choi, J. Kim, M. R. Shaker, W. Sun, J.-H. Park, D. Kim, W. D. Heo, C. Choi, *Nat. Commun.* **2016**, *7*, 12277.

[7] a) D. L. Sellers, J. M. Bergen, R. N. Johnson, H. Back, J. M. Ravits, P. J. Horner, S. H. Pun, *Proc. Natl. Acad. Sci. USA* **2016**, *113*, 2514; b) J. Chen, Y. Zou, C. Deng, F. Meng, J. Zhang, Z. Zhong, *Chem. Mater.* **2016**, *28*, 8792; c) J. d. A. Pachioni-Vasconcelos, A. M. Lopes, A. C. Apolinario, J. K. Valenzuela-Oses, J. S. R. Costa, L. d. O. Nascimento, A. Pessoa, L. R. S. Barbosa, C. d. O. Rangel-Yagui, *Biomater. Sci.* **2016**, *4*, 205; d) T. Liu, L. Lai, Z. Song, T. Chen, *Adv. Funct. Mater.* **2016**, *26*, 7775; e) G. Yang, X. Sun, J. Liu, L. Feng, Z. Liu, *Adv. Funct. Mater.* **2016**, *26*, 4722; f) X. Wei, Y. Wang, X. Xiong, X. Guo, L. Zhang, X. Zhang, S. Zhou, *Adv. Funct. Mater.* **2016**, *26*, 8266.

[8] a) S. Sonotaki, T. Takami, K. Noguchi, M. Odaka, M. Yohda, Y. Murakami, *Biomater. Sci.* **2017**, *5*, 1082; b) X. Liang, Y. Li, X. Li, L. Jing, Z. Deng, X. Yue, C. Li, Z. Dai, *Adv. Funct. Mater.* **2015**, *25*, 1451; c) L. Cheng, D. Jiang, A. Kamkaew, H. F. Valdovinos, H.-J. Im, L. Feng, C. G. England, S. Goel, T. E. Barnhart, Z. Liu, W. Cai, *Adv. Funct. Mater.* **2017**, *27*, 1702928.

[9] a) H. S. Choi, *Nat. Nanotechnol.* **2014**, *9*, 93; b) B. Pelaz, P. del Pino, P. Maffre, R. Hartmann, M. Gallego, S. Rivera-Fernandez,

J. M. de la Fuente, G. U. Nienhaus, W. J. Parak, *ACS Nano* **2015**, *9*, 6996.

[10] a) T. Jiang, R. Mo, A. Bellotti, J. Zhou, Z. Gu, *Adv. Funct. Mater.* **2014**, *24*, 2295; b) T. Akagi, F. Shima, M. Akashi, *Biomaterials* **2011**, *32*, 4959.

[11] M. R. Battig, B. Soontornworajit, Y. Wang, *J. Am. Chem. Soc.* **2012**, *134*, 12410.

[12] M. Wang, K. Alberti, S. Sun, C. L. Arellano, Q. Xu, *Angew. Chem., Int. Ed.* **2014**, *53*, 2893.

[13] M. Wang, S. Sun, C. I. Neufeld, B. Perez-Ramirez, Q. Xu, *Angew. Chem., Int. Ed.* **2014**, *53*, 13444.

[14] a) M. S. Shim, Y. Xia, *Angew. Chem., Int. Ed.* **2013**, *52*, 6926; b) C. Tapeinos, A. Pandit, *Adv. Mater.* **2016**, *28*, 5334.

[15] a) C. W. Riggsbee, A. Deiters, *Trends Biotechnol.* **2010**, *28*, 468; b) G. Miesenboeck, *Annu. Rev. Cell Dev. Biol.* **2011**, *27*, 731.

[16] a) K. M. Schelkle, T. Griesbaum, D. Ollech, S. Becht, T. Buckup, M. Hamburger, R. Wombacher, *Angew. Chem., Int. Ed.* **2015**, *54*, 2825; b) X. Chen, S. Tang, J.-S. Zheng, R. Zhao, Z.-P. Wang, W. Shao, H.-N. Chang, J.-Y. Cheng, H. Zhao, L. Liu, H. Qi, *Nat. Commun.* **2015**, *6*, 7220.

[17] a) H.-D. Gao, P. Thanasekaran, C.-W. Chiang, J.-L. Hong, Y.-C. Liu, Y.-H. Chang, H.-M. Lee, *ACS Nano* **2015**, *9*, 7041; b) S. Hauke, A. von Appen, T. Quidwai, J. Ries, R. Wombacher, *Chem. Sci.* **2017**, *8*, 559.

[18] a) H. Li, X. Fan, X. Chen, *ACS Appl. Mater. Interfaces* **2016**, *8*, 4500; b) J. Wang, Y. Wei, X. Hu, Y.-Y. Fang, X. Li, J. Liu, S. Wang, Q. Yuan, *J. Am. Chem. Soc.* **2015**, *137*, 10576.

[19] J. E. Lee, R. T. Raines, *Biodrugs* **2008**, *22*, 53.

[20] a) J. F. Lovell, T. W. B. Liu, J. Chen, G. Zheng, *Chem. Rev.* **2010**, *110*, 2839; b) J. P. Celli, B. Q. Spring, I. Rizvi, C. L. Evans, K. S. Samkoe, S. Verma, B. W. Pogue, T. Hasan, *Chem. Rev.* **2010**, *110*, 2795; c) N. M. Idris, M. K. Gnanasammandhan, J. Zhang, P. C. Ho, R. Mahendran, Y. Zhang, *Nat. Med.* **2012**, *18*, 1580; d) K. Liu, R. Xing, Q. Zou, G. Ma, H. Mohwald, X. Yan, *Angew. Chem., Int. Ed.* **2016**, *55*, 3036; e) H. Huang, B. Yu, P. Zhang, J. Huang, Y. Chen, G. Gasser, L. Ji, H. Chao, *Angew. Chem., Int. Ed.* **2015**, *54*, 14049; f) B. Cu, H. Wu, G. Xu, G. Feng, F. Yin, P. H. J. Chong, J. Qu, K.-T. Yong, B. Liu, *Adv. Mater.* **2017**, *29*, 1701076; g) W.-H. Chen, G.-F. Luo, W.-X. Qiu, Q. Lei, L.-H. Liu, S.-B. Wang, X.-Z. Zhang, *Biomaterials* **2017**, *117*, 54.

[21] G. Springsteen, B. H. Wang, *Chem. Commun.* **2001**, *17*, 1608.

[22] a) L. Yin, Z. Song, K. H. Kim, N. Zheng, N. P. Gabrielson, J. Cheng, *Adv. Mater.* **2013**, *25*, 3063; b) J. Lv, X. Hao, Q. Li, M. Akpanyung, A. Nejjari, A. L. Neve, X. Ren, Y. Feng, C. Shi, W. Zhang, *Biomater. Sci.* **2017**, *5*, 511; c) Q. Deng, X. Li, L. Zhu, H. He, D. Chen, Y. Chen, L. Yin, *Biomater. Sci.* **2017**, *5*, 1174.

[23] K. Han, W.-Y. Zhang, J. Zhang, Q. Lei, S.-B. Wang, J.-W. Liu, X.-Z. Zhang, H.-Y. Han, *Adv. Funct. Mater.* **2016**, *26*, 4351.

[24] H. He, Y. Bai, J. Wang, Q. Deng, L. Zhu, F. Meng, Z. Zhong, L. Yin, *Biomacromolecules* **2015**, *16*, 1390.

[25] K. E. Broaders, S. Grandhe, J. M. Fréchet, *J. Am. Chem. Soc.* **2010**, *133*, 756.

[26] J. L. Major Jourden, S. M. Cohen, *Angew. Chem., Int. Ed.* **2010**, *49*, 6795.

[27] J. Yang, B. Wang, Y. Liu, K. Wang, W. Xing, C. Liu, *J. Power Sources* **2014**, *248*, 660.

[28] T.-C. Chou, *Pharmacol. Rev.* **2006**, *58*, 621.